scientific reports

Check for updates

OPEN

Chitosan hydrogel/silk fibroin/$Mg(OH)_2$ nanobiocomposite as a novel scaffold with antimicrobial activity and improved mechanical properties

Reza Eivazzadeh-Keihan[1], Fateme Radinekiyan[1], Hooman Aghamirza Moghim Aliabadi[2,3], Sima Sukhtezari[1], Behnam Tahmasebi[4], Ali Maleki[1]✉ & Hamid Madanchi[5,6]✉

Herein, a novel nanobiocomposite scaffold based on modifying synthesized cross-linked terephthaloyl thiourea-chitosan hydrogel (CTT-CS hydrogel) substrate using the extracted silk fibroin (SF) biopolymer and prepared $Mg(OH)_2$ nanoparticles was designed and synthesized. The biological capacity of this nanobiocomposite scaffold was evaluated by cell viability method, red blood cells hemolytic and anti-biofilm assays. According to the obtained results from 3 and 7 days, the cell viability of CTT-CS/SF/$Mg(OH)_2$ nanobiocomposite scaffold was accompanied by a considerable increment from 62.5 to 89.6% respectively. Furthermore, its low hemolytic effect (4.5%), and as well, the high anti-biofilm activity and prevention of the *P. aeruginosa* biofilm formation confirmed its promising hemocompatibility and antibacterial activity. Apart from the cell viability, blood biocompatibility, and antibacterial activity of CTT-CS/SF/$Mg(OH)_2$ nanobiocomposite scaffold, its structural features were characterized using spectral and analytical techniques (FT-IR, EDX, FE-SEM and TG). As well as, given the mechanical tests, it was indicated that the addition of SF and $Mg(OH)_2$ nanoparticles to the CTT-CS hydrogel could improve its compressive strength from 65.42 to 649.56 kPa.

One of the most remarkable therapeutic perspectives in regenerative medicine technologies is biological wound healing approach. Series of molecular and cellular events are performed in tissue repair and regeneration processes in order to restore tissue damages. Haemostasis, inflammation, proliferative phase, and tissue remodelling phase are defined as the sequential steps of tissue regeneration. On top of that, these biochemical events are subsequently associated with the integrated and dynamic activities of soluble mediators, red blood cells (RBCs), and parenchymal cells[1]. In this research area, many substantial features such as having similarity to the human extracellular matrix (ECM) and excellent hemocompatibility are the consequential factors in designing novel biomedical scaffolds. Besides, two main structural features including the engineered porosity for cellular ingrowth and vascularization and as well, the supportive architecture for cellular migration and proliferation, must be considered[2].

Up to now, biocompatible and natural polymers have been indicated high efficient performances in developing catalysis science[3,4] and biomedical fields; especially in drug delivery, tissue engineering, and wound healing[5,6]. These natural structures in the form of macromolecular hydrogel networks can act as soft tissue-like structures

[1]Catalysts and Organic Synthesis Research Laboratory, Department of Chemistry, Iran University of Science and Technology, 16846-13114 Tehran, Iran. [2]Faculty of Chemistry, K.N. Toosi University of Technology, Tehran, Iran. [3]Protein Chemistry Laboratory, Department of Medical Biotechnology, Biotechnology Research Center, Pasteur Institute of Iran, Tehran, Iran. [4]School of Chemistry, College of Science, University of Tehran, Tehran, Iran. [5]Department of Biotechnology, School of Medicine, Semnan University of Medical Sciences, Semnan, Iran. [6]Drug Design and Bioinformatics Unit, Department of Medical Biotechnology, Biotechnology Research Center, Pasteur Institute of Iran, Tehran, Iran. ✉email: maleki@iust.ac.ir; hamidmadanchi@yahoo.com

due to their hydrophilic nature, high sensitivity to the physiological environments, adequate flexibility and adsorptive capacity for large amount of water and biological fluids[7,8]. Given these unique features, an appropriate wound healing environment can be provided by protective hydrogel-based wound care dressing. So far, the efficiency and excellent potential of natural polymers have been approved in the synthesis of a wide range of hydrogel-based scaffolds. Chitosan (CS) as a cationic natural polysaccharide which has a structural similarity to glycosaminoglycans, is one of the promising biocompatible materials in wound and tissue repair[9,10]. Apart from its unique biological features including antibacterial, antifungal, mucoadhesive, analgesic properties and also, the hemostasis simulation and function modulation of inflammatory cells[11–14], its bioactive *N*-acetyl-b-D-glucosamine monomeric units can enhance the synthesis process of extracellular hyaluronic acid and fibroblast proliferation. Furthermore, these units can simplify the deposition of ordered collagen at damaged wound sites[9]. Chitosan has low solubility in neutral and alkaline solutions which, limits its application. However, its physical and chemical modifications and formation of new cross-linked chitosan-based structures, have provided unique functional properties for extensive use in biosensing[15,16], tissue engineering[17], and pharmaceutical fields[18]. In other words, given the chitosan structure, its reactive amino and hydroxyl functional groups can react covalently or no-covalently with various cross-linker reagents such as glutaraldehyde[19], genipine[20], acrylic acid[21], and palladium cations[22]. In fact, these cross-linking reactions led to generate new cross-linked chitosan-based composites and hydrogels with different performances[18,23]. Alongside natural polysaccharides, natural proteins are one of the sophisticated groups, which have been captured the imagination of scientists due to their substantial potential use in biomedical fields[24,25]. In this regard, silk fibroin (SF) has been highlighted because of its unique features such as robust mechanical strength, low immunogenicity, non-cytotoxicity, non-carcinogenic, and haemostatic properties[26,27]. Furthermore, the exceptional biocompatibility of SF with a diversity of cells and tissues, and also, its efficient potential in promoting cellular adhesion and proliferation of fibroblasts and keratinocytes have been approved[27–29]. This natural protein can be formed in different material shape and structures such as hydrogel[30], film[31], nonwoven fabrics[32], nanofiber[33], and 3D porous scaffolds[34]. However, alongside its super mechanical property, studies have been indicated that its combination with other materials such as graphene oxide[35], natural polymers[28,36], metal nanoparticles[37,38], and the formation of SF-based composite can enhance the antimicrobial property of SF; which is essential factor for wound dressing use. Following these descriptions, in recent years, according to the unique physicochemical and fascinating biomedical features of nano materials, their synthesis and application have been extended exclusively[39]. Research studies have been determined that nano materials can be applied in functional composites, catalysts, sensors, semiconductors, microelectronics and as well, medical use[39]. In this context, the development of biocompatible magnesium hydroxide nanoparticles ($Mg(OH)_2$ NPs) as potent antibacterial and antifungal agents have been attracted great interests of scientists[40]. These nano-scale particles can be efficiently used in pharmaceutical formulations[41–43]. Furthermore, the antimicrobial studies of $Mg(OH)_2$ NPs have indicated that the in-vivo toxicity of these particles are low and in sensible amounts, they show non-toxic effect on humans[44]. In this present study, a new cross-linked terephthaloyl thiourea-chitosan/silk fibroin/$Mg(OH)_2$ (CTT-CS/SF/$Mg(OH)_2$) nanobiocomposite scaffold is introduced due to considering the modification process of synthesized cross-linked terephthaloyl thiourea-chitosan hydrogel (CTT-CS hydrogel) by extracted SF solution (CTT-CS/SF hydrogel) and using synthesized $Mg(OH)_2$ NPs in order to improve its antibacterial activity (Fig. 1). Different spectral and analytical techniques including FT-IR, EDX, FE-SEM, TG analyses and as well, the mechanical tests were taken. The obtained results were evaluated to characterize the unique structural features of CTT-CS/SF/$Mg(OH)_2$ nanobiocomposite scaffold. After the structural characterization, the cytotoxicity and accessibility of cellular metabolic activity of this synthetic nanobiocomposite scaffold were studied by 3-(4,5-dimethyl-2-thiazolyl)-2,5-diphenyl-2H-tetrazolium bromide (MTT) assay using Hu02 cell lines in 3 and 7 days. Following the MTT assay results, the RBCs hemolytic assay was conducted to determine its in-vitro blood biocompatibility and hemolytic effect. Besides, the antibacterial activity of this synthetic nanobiocomposite was evaluated by anti-biofilm assay.

Experimental

Materials. Apart from silk worm cocoons, all of the needed chemical materials including chemical reagents and chemical solvents with high purities were procured in advance from international companies, Sigma-Aldrich, and Fluka.

Fourier-transform infrared spectroscopy. All of the spectra were taken using Fourier-transform infrared (FT-IR) spectrometer (Shimadzu FT-8400s model, Japan) in order to characterize the functional groups in each synthesis step. To prepare the sample pellets, 0.1–1.0% of each sample was well mixed into 200–250 mg of fine KBr powder. The spectral resolution was 4 cm^{-1} in 400–4000 cm^{-1} frequency range. As well, all of the spectra were taken at room temperature and the average number of scans was between 6 to 18[45].

Energy-dispersive X-ray spectroscopy. The elemental composition of sample was characterized by energy-dispersive X-ray (EDX) device (SAMx model, France) and ultrathin window detector. Besides, the distribution pattern of elemental composition was determined by elemental mapping images.

Field-emission scanning microscopy. The morphology and structure of all samples were visualized using the field-emission scanning microscope (FE-SEM) (ZEISS-Sigma VP model, Germany), operating at a 15 kV. Each sample was mounted with double side carbon tape on stainless steel stub, and they were sputter-coated with gold (Agar Sputter Coater model, Agar Scientific, England)[45].

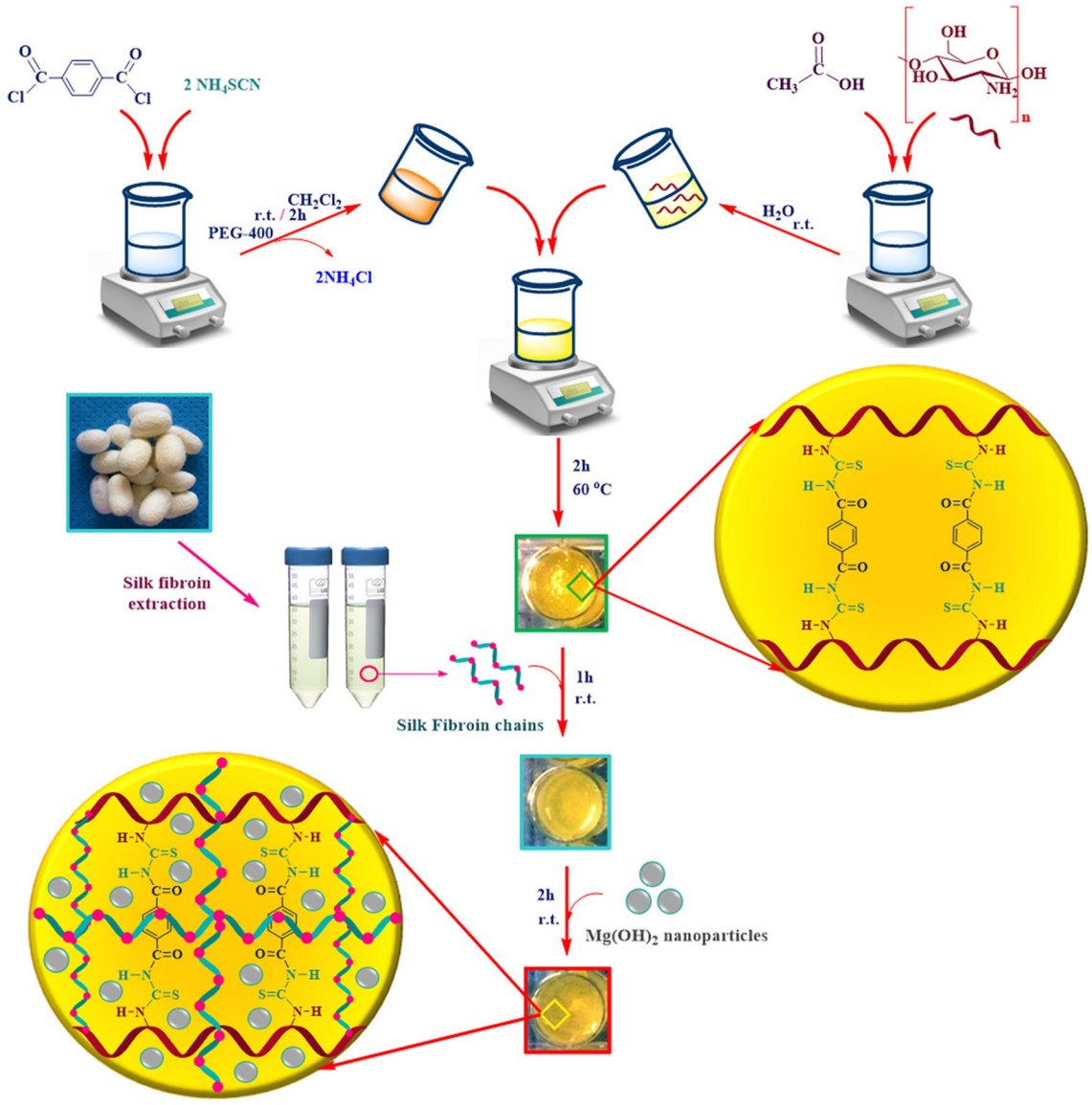

Figure 1. Synthesis preparation of CTT-CS/SF/$Mg(OH)_2$ nanobiocomposite scaffold.

Thermogravimetric analysis. The thermogravimetric (TG) analysis was conducted by using Bahr-STA 504 instrument (Germany). The analysis was performed with 5.0 mg of sample in alumina pans under the argon atmosphere. The argon flow rate was 1 L/h; also, each thermal cycle was run between 50 to 800 °C with a constant heating rate (10 °C/min)[45].

Compressive mechanical properties. The compressive mechanical properties of scaffolds were measured according to the procedure of Bhardwaj et al., and ASTM method F451-95 with some modifications[46]. The mechanical tests were performed using a universal testing machine (SANTAM, STM-20 model, Iran) with crosshead speed 1 mm/min at room temperature. In this test, first, the sample scaffolds with a thickness of 10 mm and a diameter of 13 mm were manually cut using a razor blade. Then, the samples were soaked in phosphate-buffered saline (PBS) solution for 2 h and the related tests were conducted under wet conditions. For each sample, at least three fragments were tested and the mean values were reported.

In-vitro cytotoxicity assay. MTT assay was performed to evaluate the biocompatibility and cell viability of CTT-CS/SF/$Mg(OH)_2$ nanobiocomposite scaffold. For this purpose, Hu02 cell line (human skin fibroblast cells) was cultured at 1×10^5 cell/well in 96 well plate on the scaffold in the optimal conditions (37 °C, 5% CO_2 in humidified incubator) for 3 and 7 days. Cultured cells in a culture plate containing cisplatin were then considered as a positive control and the rate of cells proliferation on the scaffold was compared with this positive control. Attached Roswell park memorial institute medium (RPMI) without scaffold and cells in each well, was also considered as negative control. In the following, the 5 mg/mL of 3-(4,5-dimethyl-2-thiazolyl)-2,5-diphenyl-2H-tetrazolium bromide in phosphate-buffered saline (PBS) solution was freshly prepared. Then, 10 µL of pre-

pared solution was added to each well and the cells were treated with this solution at 37 °C for 4 h. Thereafter, the media with MTT solution was removed and 100 µL of 2-propanol was added to each well. Next, the plates were gently shaken to simplify solubilization of formazan crystal[47]. Finally, using a microplate reader (STAT FAX 2100, BioTek, Winooski, USA), the absorbance of each well was measured at 590 nm, and the percentage of toxicity and cell viability were calculated using following Eqs. (1–2).

$$\text{Toxicity (\%)} = \left(1 - \frac{\text{mean OD of sample}}{\text{mean OD of control}}\right) \times 100 \quad (1)$$

$$\text{Cell viability (\%)} = 100\ (\%) - \text{Toxicity (\%)} \quad (2)$$

In-vitro hemocompatibility assay. Hemolytic assay was used to determine the blood compatibility of the CTT-CS/SF/$Mg(OH)_2$ nanobiocomposite scaffold on human red blood cells (RBCs) and as well measuring its potential lytic effects. A volunteer with O blood type was first selected and after completing informed consent form, fresh blood samples were taken from him and then, a 15% v/v suspension of human RBCs was prepared in 0.9% NaCl solution. The experimental procedures and the procedure for obtaining informed consent were approved by Semnan university of medical sciences, ethics research committee (Approved ID: IR.SEMUMS.REC.1399.159) and the study was conducted in accordance with the principles outlined in the declaration of Helsinki. Subsequently, determined pieces of CTT-CS hydrogel, CTT-CS/SF hydrogel and CTT-CS/SF/$Mg(OH)_2$ nanobiocomposite scaffold (4 mm × 4 mm) were placed in a 96-well plate and 100 µL of the suspension was added to each well. Also, 1% Triton X-100 solution and 0.9% sterile NaCl solution were respectively used as positive control for 100% lysis of erythrocytes and negative control. In this test, each treatment was repeated three times[48]. In the following, the plate was incubated at 37 °C for 1 h and then centrifuged for 10 min at 3500 rpm. After centrifugation, 150 µL of the supernatant was transferred to a new 96-well plate to evaluate the absorbance at 414 nm using a microplate reader (STAT FAX 2100, BioTek, Winooski, USA). Eventually, the hemolysis percentage of the samples was calculated using the following Eq. (3).

$$\text{Hemolysis (\%)} = \left(\frac{\text{mean OD of sample} - \text{mean OD of negative sample}}{\text{mean OD of positive control} - \text{mean OD of negative control}}\right) \times 100 \quad (3)$$

Anti-biofilm assay. The antimicrobial properties of the CTT-CS/SF/$Mg(OH)_2$ nanobiocomposite scaffold were analysed using a tissue culture plate (TCP) anti-biofilm assay with some corrections[49]. For this purpose, determined fragments of CTT-CS hydrogel, CTT-CS/SF hydrogel, designed nanobiocomposite scaffold (1 cm^2) and a polystyrene piece (as a positive control) were sterilized in 70% ethanol aqueous solution, and then dried in a sterilized incubator at 37 °C. Subsequently, each piece was placed in a sterilized tube containing selected bacteria (*Pseudomonas aeruginosa* ATCC 27853) at concentration of 107 colony-forming unit (CFU)/mL in nutrient broth (NB) culture medium. All three tubes were then incubated in a shaker incubator with shake speed 150 rpm at 37 °C for 24 h. After shaking, samples were removed from the tubes and washed twice by PBS solution. To evaluate the anti-biofilm properties of the nanobiocomposite scaffold, all three samples were stained by 0.1% crystal violet solution for 5 min and then washed by 33% acetic acid solution to separate the bacteria from their surface. Eventually, using a microplate reader (STAT FAX 2100, BioTek, Winooski, USA), the absorbance of the finishing solutions was evaluated at 570 nm.

Statistical analysis. The statistical analysis was used to compare the in-vitro cytotoxicity, in-vitro hemocompatibility, and anti-biofilm assays results. This analysis was conducted by a t-test by SPSS Statistics 22.0 software (SPSS Inc., Chicago, IL, USA). The P values of < 0.05 were considered as statistically significant.

Preparation of CTT-CS hydrogel. Taking into account the previous studies about the synthesis of cross-linked terephthaloyl thiourea-chitosan hydrogel as antibacterial and antifungal agents[50] and as well as, designing magnetic nanocomposite based on this efficient cross-linked chitosan hydrogel substrate[51], the synthesis of CTT-CS hydrogel was accomplished by following these synthesis steps. First of all, distinctive amounts of ammonium thiocyanate (20 mmol) and terephthaloyl chloride (10 mmol) were separately dissolved in 20 mL of dichloromethane. Afterwards, the prepared terephthaloyl chloride solution was drop wisely added to the ammonium thiocyanate solution which was kept under the stirring condition. Following the addition of terephthaloyl chloride solution, 1 mL of polyethylene glycol-400 as phase transfer catalyst was added to the reaction mixture. Then, the whole mixture solution was stirred for 2 h at room temperature condition. After the mentioned time (2 h) and formation of white precipitate of ammonium chloride, the yellow mixture solution was filtered in order to remove the ammonium chloride. In the next step, the yellow transparent solution which was obtained from the filtration process was added to distinctive concentration of chitosan solution (3.22 g of chitosan powder in 200 mL of acetic acid solution (1%)). Afterwards, the reaction mixture was mechanically stirred for 2 h in a determined thermal condition (60 °C). After the mentioned time in a constant thermal condition (60 °C) and cooling process, the homogenous cross-linked chitosan hydrogel was neutralized with saturated solution of sodium carbonate (pH = 7). As well as, the obtained cross-linked hydrogel product was submerged in methanol for 24 h to dewater completely. Following the dewatering process, the neutralized CTT-CS hydrogel was poured into petri dish and it was kept at − 70 °C for 24 h for pre-preparing freeze-drying process. After the mentioned time, the freezed petri dish was put in to the freeze-dryer device (shelve) in order to accomplish the solvent sub-

limation process during 24 h. Besides, it should be mentioned that this dehydration process was conducted due to considering determined temperature condition (− 60 °C) and 0.1 bar pressure.

Extraction process of SF. Conforming to the previous studies about the degumming treatment methods and extraction of silk fibroin[45,52,53], first, the silkworm cocoons were cut in to small pieces. Afterwards, in a determined aqueous solution of Na_2CO_3 (0.21% w/v), the cocoon pieces were boiled during 2 h in order to remove the glue like sericin proteins from the cocoon structure. Following the mentioned time (2 h), the degummed silk fibers were eluted several times with distilled water. Then, the eluted fibers were dried for an overnight at room temperature. In the next step, the dried silk fibers were dissolved in an appropriate concentration of LiBr solution (9.3 M) and the solution was kept under the stirring condition for 2 h. Subsequently, to remove the excess amount of LiBr and other impurities, the clear obtained solution from previous step was poured into dialysis tubing cellulose membrane for preparing the dialysis process in the presence of distilled water. The dialysis process was continued for three days at room temperature condition. After three days, the purified silk fibroin solution was egressed from the dialysis tube membrane and it was kept at 4 °C for the next synthesis step.

Preparation of $Mg(OH)_2$ NPs. According to the previous studies with some modifications[54], first, 250 mL of aqueous $MgSO_4$ solution (0.2 M) was added to the 250 mL of NaOH solution (0.4 M) under the continuous stirring condition at room temperature (25 °C). After 1 h, the white $Mg(OH)_2$ precipitate was centrifuged and subsequently, it was washed with distilled water and 2-propanol. In order to remove the by-product of reaction (Na_2SO_4), the centrifugation and washing processes were repeated five times. Afterwards, the $Mg(OH)_2$ NPs were dried at room temperature for 24 h. Finally, the dried white powder was prepared for the next synthesis step.

Modification of CTT-CS hydrogel by extracted SF. According to previous research works and some corrections[45,55], to modify the CTT-CS hydrogel, in a small scale, 0.6 mL of SF solution was added to the 0.6 mL of CTT-CS hydrogel solution. Two mentioned solutions were mixed and kept under the stirring condition for 1 h. After the mentioned time, to pre-prepare the suspension mixture for freeze-drying process, the obtained CTT-CS/SF hydrogel was poured into a petri dish and it was kept at freezer (− 70 °C) for 24 h. Afterwards, the freezed petri dish was put in to the freeze-dryer device (shelve) in order to conduct the solvent sublimation process during 24 h. In addition, it should be mentioned that this dehydration process was conducted due to considering a determined temperature condition (− 60 °C) and 0.1 bar pressure.

Preparation of CTT-CS/SF/$Mg(OH)_2$ nanobiocomposite scaffold by CTT-CS/SF hydrogel and addition of $Mg(OH)_2$ NPs. Based on the excellent antibacterial activity of $Mg(OH)_2$ nanostructures, to enhance the antibacterial activity of CTT-CS/SF hydrogel, with some modifications[55], again, in a small scale 0.3% w/w of synthesized $Mg(OH)_2$ NPs were added to a determined amount of modified cross-linked hydrogel (1.2 mL). Next, the intended suspension mixture was kept under the stirring condition at room temperature for 2 h. After the mentioned time, the obtained homogenous suspension compound was poured into petri dish and like the previous synthesis steps, to pre-prepare it for freeze-drying process, it was kept in the freezer (− 70 °C) for 24 h.

Results and discussion

In this present study, based on substantial importance of unique regenerative medicine strategies and dynamic wound healing approaches, novel CTT-CS/SF/$Mg(OH)_2$ nanobiocomposite scaffold was designed and synthesized due to modifying CTT-CS hydrogel using extracted SF and presence of synthesized $Mg(OH)_2$ NPs. The cytotoxicity effect of this biocompatible scaffold was evaluated in the presence of Hu02 cell lines. Its antibacterial activity was examined by anti-biofilm assay. Besides, its in-vitro blood biocompatibility and effective hemolytic impact on erythrocyte cells were approved by RBCs hemolytic assay. As could be illustrated in Fig. 1, the synthesis preparation of designed CTT-CS/SF/$Mg(OH)_2$ nanobiocomposite scaffold is conducted in three main synthesis steps. The first step is the formation of CTT-CS hydrogel substrate. In the second step, the modification process of the cross-linked chitosan hydrogel is conducted using extracted SF solution. Finally, in order to improve the antibacterial activity of CTT-CS/SF hydrogel and synthesize novel CTT-CS/SF/$Mg(OH)_2$ nanobiocomposite scaffold, the prepared $Mg(OH)_2$ NPs were added to the related modified cross-linked hydrogel. Alongside the synthesis preparation of this efficient nanobiocomposite scaffold, its unique structural features were characterized using various spectral and analytical detection techniques. In this respect, the formation and presence of new chemical bonds and functional groups were determined by FT-IR spectra. The structural elements were identified using EDX analysis. As well as, the distribution of structural elements was evaluated by chemical elemental mapping. The FE-SEM imaging disclosed a different structural morphology in each synthesis step. In addition, the thermogravimetric behavior of designed CTT-CS/SF/$Mg(OH)_2$ nanobiocomposite scaffold was investigated by TG analysis. In this section, the characteristic evaluation of synthetic nanobiocomposite scaffold is described respectively.

Characterization of CTT-CS/SF/$Mg(OH)_2$ nanobiocomposite scaffold. *FT-IR analysis.* The formation of CTT-CS/SF/$Mg(OH)_2$ nanobiocomposite scaffold was evaluated by characterizing the FT-IR spectrum obtained from each synthesis step (Fig. 2a–c). Due to considering the FT-IR spectrum of chitosan biopolymer (Fig. 2a), apart from the intermolecular hydrogen bonds of this biopolymer, the stretching vibration modes of N–H and O–H bonds were determined by observing a broad and strong band at the region of 3200–3600 cm^{-1}[56].

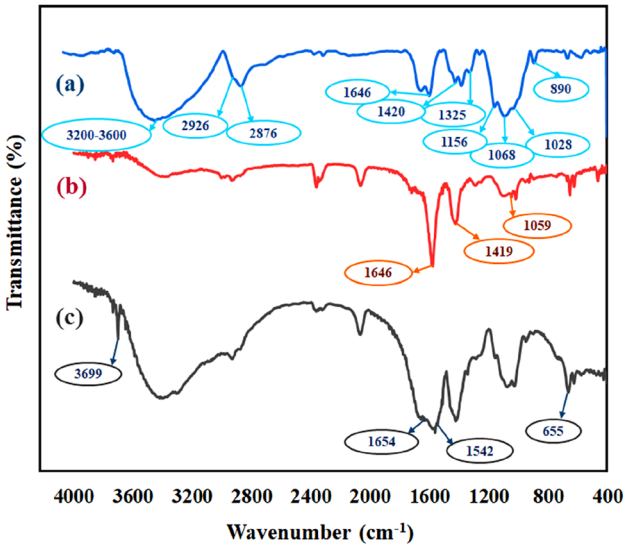

Figure 2. FT-IR spectra of (**a**) chitosan biopolymer, (**b**) CTT-CS hydrogel, (**c**) CTT-CS/SF/$Mg(OH)_2$ nanobiocomposite scaffold.

The C–H bending out of plane which was related to the monosaccharide ring and as well, the symmetric and asymmetric vibration modes of C–H bonds were characterized by observing three absorption bands around 890 cm^{-1}, 2926 cm^{-1}, and 2876 cm^{-1}[156]. Assigning a small absorption band around 1325 cm^{-1} was attributed to the C–N stretching vibration mode of amide III and as well, its carbonyl stretching vibration mode of amide I was indicated by characterizing a strong absorption band around 1646 cm^{-1}[156]. Observing two strong absorption bands around 1068 cm^{-1} and 1028 cm^{-1} was ascribed to the stretching vibration mode of C–O bond[56]. In addition, the stretching vibration mode of C–O–C bridge bond and bending vibration mode of CH_2 group were characterized by observing two absorption bands around 1156 cm^{-1} and 1420 cm^{-1}[156]. Following characterizing the FT-IR spectrum of chitosan biopolymer, the formation of cross-linked terephthaloyl thiourea-chitosan hydrogel was confirmed by FT-IR spectrum due to assigning new absorption bands (Fig. 2b). As could be illustrated in Fig. 2b, a sharp absorption band around 1646 cm^{-1} was attributed to the overlapped carbonyl bond (C=O) and C=C bond of phenyl and as well, N–H bond of amine (II)[50]. The –N–C–S– bending vibration mode and C=S stretching vibration mode were assigned due to observing almost strong absorption band at 1419 cm^{-1} and an absorption band at 1059 cm^{-1}[150]. Apart from new absorption bands, in comparison to FT-IR spectrum of chitosan biopolymer (Fig. 2a), it is disclosed that the intensity of broad absorption band at region of 3200–3600 cm^{-1} has reduced. This reduction can be attributed to the reaction accomplishment of amine group of chitosan biopolymer and synthetic terephthaloyl diisothiocyanate[50]. Following the mentioned explanations, the FT-IR spectrum of CTT-CS/SF/$Mg(OH)_2$ nanobiocomposite scaffold is determined in Fig. 2c. Mainly, the conformation of SF proteins can be identified by three vibrational bands in different FT-IR region. C–N stretching vibration mode of amide III (1230–1270 cm^{-1}), N–H bending vibration mode of amide II (1520–1540 cm^{-1}) and as well, C=O stretching vibration mode of amide I (1630–1650 cm^{-1})[57]. According to the appearance of two absorption bands at 1542 cm^{-1} and 1654 cm^{-1}, the random coil conformation was characterized for extracted SF which was a part of CTT-CS/SF/$Mg(OH)_2$ nanobiocomposite scaffold[57]. Alongside SF characterization, the sharp and intense absorption band at 3699 cm^{-1} and a small absorption band around 655 cm^{-1} were respectively ascribed to the O–H groups and stretching vibration mode of Mg–O–Mg bond of synthesized $Mg(OH)_2$ NPs[58].

EDX analysis. According to the EDX analysis as a qualitative detection technique for structural elements of a diversity of compounds, the EDX analysis results of synthesized CTT-CS/SF/$Mg(OH)_2$ nanobiocomposite scaffold are well indicated in Fig. 3a–b. As could be observed in the resulted EDX spectrum (Fig. 3a), the presence of two sulfur peaks was attributed to the synthetic terephthaloyl diisothiocyanate cross-linker. The presence of related organic structures including chitosan biopolymer and SF protein was characterized by observing three strong carbon, oxygen and nitrogen peaks. Besides, the observed magnesium peak was confirmed the presence of $Mg(OH)_2$ NPs. In addition, it should be mentioned that the presence of sodium peak can be ascribed to the neutralization process of synthesized CTT-CS hydrogel which was conducted by saturation solution of sodium carbonate. Apart from the EDX spectrum and detection of related structural elements, the distribution form of mentioned elements was well indicated by elemental mapping images (Fig. 3b).

FE-SEM imaging. The surface imaging was taken from each synthesis step in order to characterize the morphology and structure. As illustrated, the FE-SEM images of CTT-CS hydrogel scaffold and its modified structure using SF (CTT-CS/SF hydrogel) are well determined in Fig. 4a–c. As can be observed, CTT-CS hydrogel structure has shown a considerable porosity with no specific morphology. Even, due to adding SF polymeric structure, this porosity has retained with no particular alternation (Fig. 4c). As well as, the FE-SEM imaging

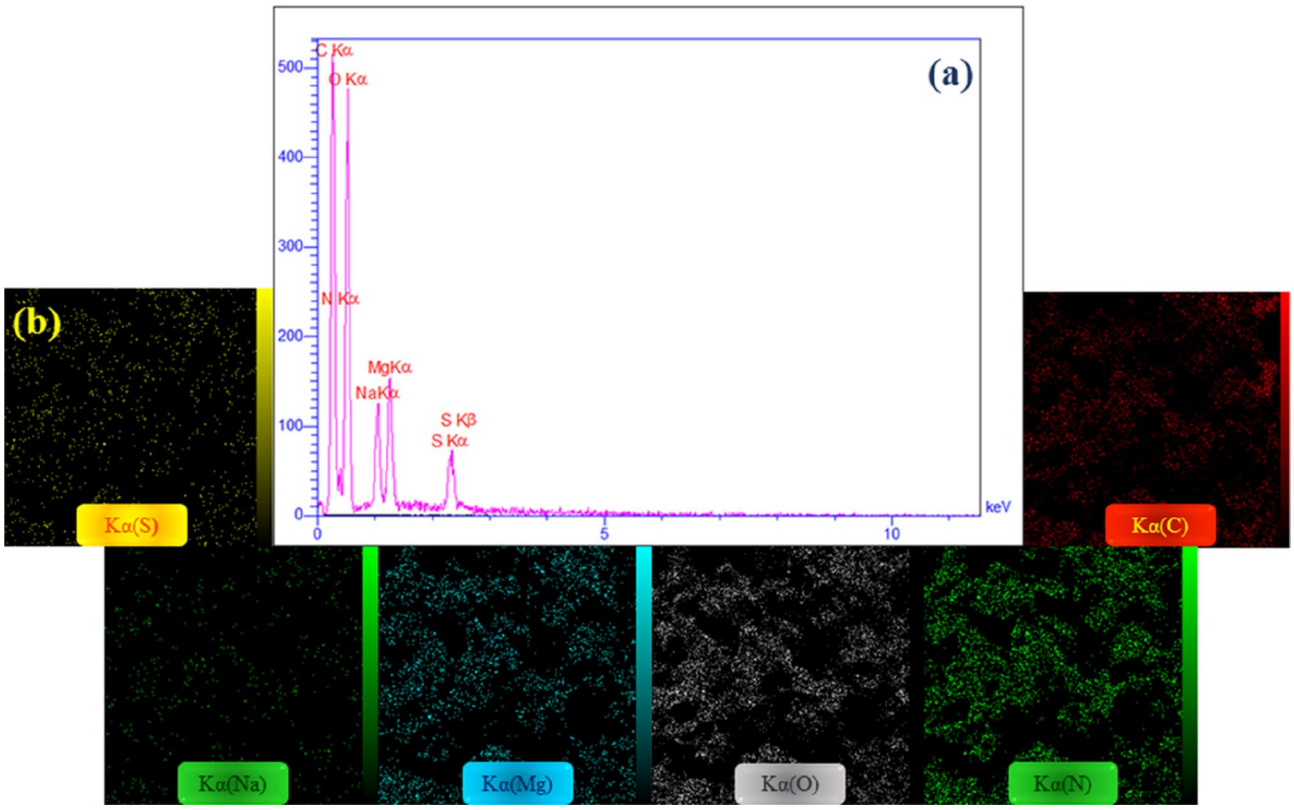

Figure 3. (**a**) EDX spectrum, (**b**) elemental mapping images of CTT-CS/SF/$Mg(OH)_2$ nanobiocomposite scaffold.

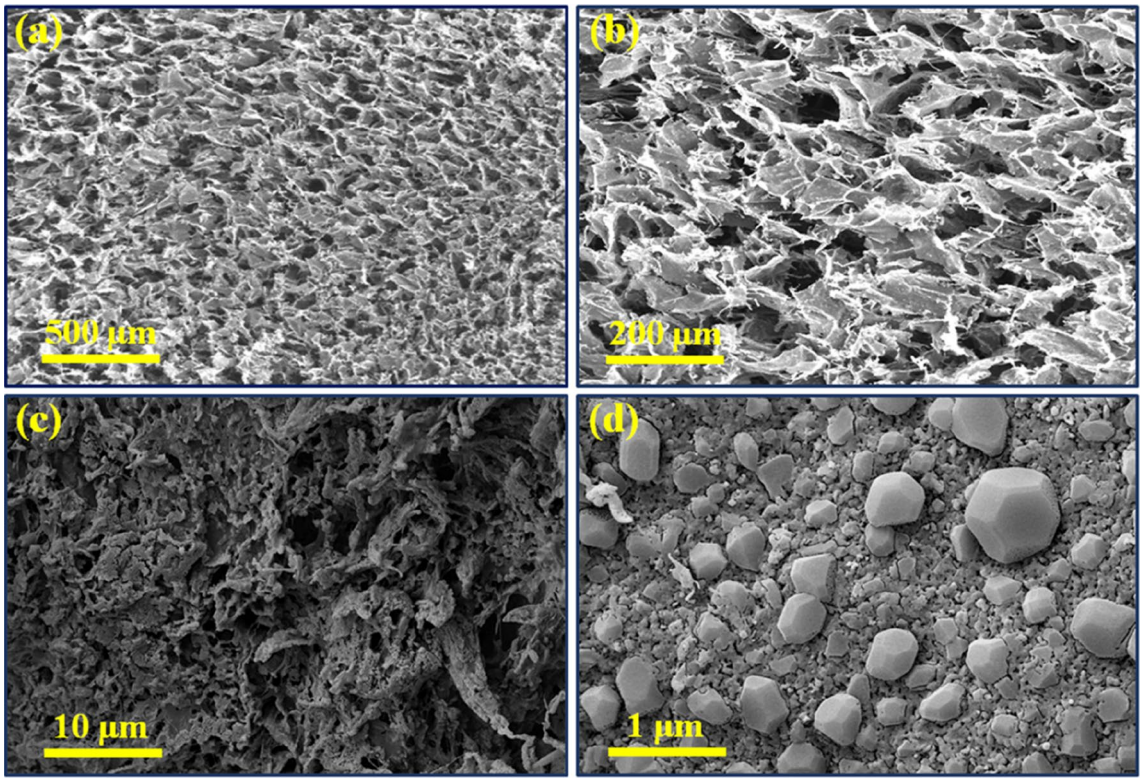

Figure 4. FE-SEM images of (**a**,**b**) CTT-CS hydrogel, (**c**) CTT-CS/SF hydrogel, (**d**) synthetic CTT-CS/SF/$Mg(OH)_2$ nanobiocomposite scaffold (freeze-dried structures).

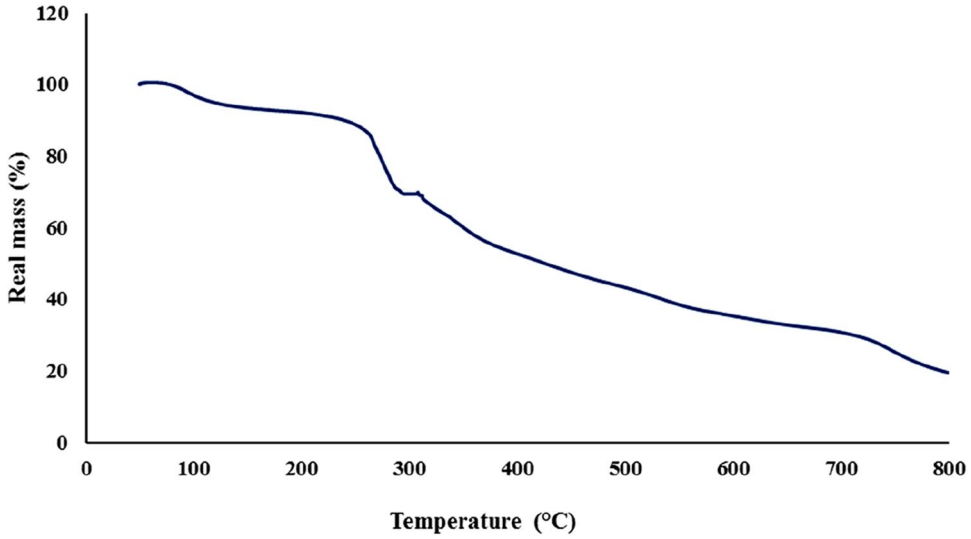

Figure 5. Thermogravimetric curve of synthetic CTT-CS/SF/$Mg(OH)_2$ nanobiocomposite scaffold.

Entry	Sample	Compressive strength (kPa)
1	Silk fibroin (SF) scaffold	151.73
2	CTT-CS hydrogel scaffold	65.42
3	CTT-CS/SF hydrogel scaffold	248.81
4	CTT-CS/SF/$Mg(OH)_2$ nanobiocomposite scaffold	649.56

Table 1. Compressive strength of synthesized scaffolds.

form the surface of CTT-CS/SF/$Mg(OH)_2$ nanobiocomposite scaffold well indicated the presence of $Mg(OH)_2$ NPs with almost sphere morphology in the nanobiocomposite structure (Fig. 4d).

Thermogravimetric analysis. The thermal stability and thermogravimetric behavior of CTT-CS/SF/$Mg(OH)_2$ nanobiocomposite scaffold were monitored by TG analysis due to the weight changes over the time and considering constant heating rate (10 °C/min) under the argon atmosphere. As could be seen in Fig. 5, the temperature increment was accompanied by different percentages of weight loss. According to the resulted thermogravimetric curve, the first mass reduction (almost 7%) at temperature range of 50 °C to approximate 130 °C was attributed to the evaporation of trapped water molecules and possible impurities. The second mass reduction (almost 22%) which was started from almost 240 °C to 300 °C, was attributed to the cleavage of peptide bonds and side chain groups of amino acid residue of silk fibroin structure[59,60]. In the following, almost 32% of mass reduction at temperature range of 310 °C to almost 600 °C was imputed to the oxidative decomposition of polymeric strands of chitosan substrate[61].

Compressive mechanical tests. The compressive strength was calculated using the following Eq. (4).

$$\sigma = F/A \tag{4}$$

where F is force, and A is area defined as the cross section of the sample[62]. Accordingly, the compressive strength of the scaffolds was obtained and the results are summarized in Table 1.

The comparative diagram of obtained results can also be seen in Fig. 6. Based on previous studies, it has indicated that chitosan hydrogels have low mechanical strength and are rapidly degraded; therefore, their use is limited in biomedical materials[63]. Besides, studies have shown that the mechanical properties of chitosan biopolymer can be increased significantly after the different chemical modification processes and also, its combination with other polymers makes it highly desirable for wound healing as a coverage material[64]. On the other hand, silk fibroin has been shown high mechanical strength[63]. Also, the addition of $Mg(OH)_2$ NPs as a filler can improve the mechanical properties of designed nanocomposites[65]. In fact, the nanoparticles could act as a reinforcing filler of the blend films and composites[63,66]. Overall, the suitability of mechanical properties in wound healing and tissue engineering is crucial. Accordingly, in this study, CTT-CS hydrogel was first synthesized. Then, the extracted SF solution and $Mg(OH)_2$ NPs were added in order to improve its mechanical strength. As illustrated in the Table 1 and Fig. 6, the compressive strength of CTT-CS hydrogel scaffold was measured 65.42 kPa. For SF scaffold, the compressive strength (151.73 kPa) was more than (two-fold) the compressive strength of CTT-CS hydrogel scaffold. The addition of SF and its combination with CTT-CS hydrogel scaffold were accompanied by

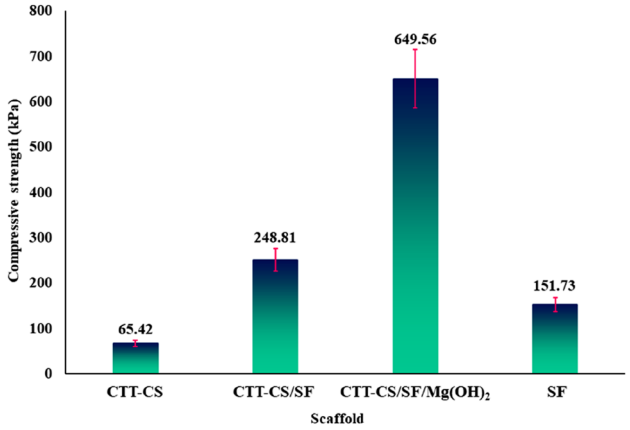

Figure 6. Compressive strength of the scaffolds from the four groups. Data represent the mean ± SD (n = 3).

considerable increment in compressive strength more than 3.5-fold (248.81 kPa). Furthermore, the addition of $Mg(OH)_2$ NPs to the CTT-CS/SF hydrogel scaffold, was increased the compressive strength (649.56 kPa) more than 2.5-fold, which could be attributed to the formation of hydrogen bonds between the $Mg(OH)_2$ NPs and the structure of hydrogel scaffold[67]. Therefore, it could be concluded that the addition of SF and $Mg(OH)_2$ NPs to the CTT-CS hydrogel could improve its compressive strength from 65.42 to 649.56 kPa, which could make it suitable scaffold for biomedical applications such as wound healing.

Bio-application of CTT-CS/SF/$Mg(OH)_2$ nanobiocomposite. *In-vitro cytotoxicity assay results.* The modern methods of wound dressing, wound healing, and as well, skin tissue engineering are the use of biocompatible scaffolds with a non-toxic nature[68]. In this study, MTT assay was used to evaluate the biocompatibility, cell viability, toxicity of the CTT-CS/SF/$Mg(OH)_2$ nanobiocomposite scaffold, and as well, its potential for use in wound healing. According to the obtained results, the viability percentage of Hu02 cells treated with CTT-CS/SF/$Mg(OH)_2$ nanobiocomposite scaffold, after 3 and 7 days was 62.5% and 89.6%, respectively; whereas, for the control group (untreated cells), this value was 95.7% and 93.2%, respectively. Statistical analysis showed that there was no significant difference between cell viability of the control group and scaffold ($P > 0.05$). Also, cisplatin at a concentration of 1 µg/mL was used as positive control. On day 3 and day 7, it killed more than 90% and 96% of cells, respectively. These results are indicated in Fig. 7a–b. Besides, it was determined that the cell viability increased with the time; which was a considerable advantage. Studies have been shown that $Mg(OH)_2$ NPs have exhibited partial toxicity to human cells[69]. Meng and co-workers showed that $Mg(OH)_2$ NPs at a concentration of 200 µg/mL, significantly inhibited the proliferation of human umbilical vein vascular endothelial cells (HUVECs)[69]. However, the MTT assay results of this study determined that the toxicity of the $Mg(OH)_2$ NPs in the structure of synthesized CTT-CS/SF/$Mg(OH)_2$ nanobiocomposite scaffold was moderated. As well as, the viability of cells in the presence of scaffold did not decrease significantly compared to the control group (untreated cells) (Fig. 7c).

In-vitro hemocompatibility results. Hemolytic assay is a very common and important test for materials that come into direct contact with blood. Blood compatibility is a crucial factor in deciding whether to use materials[70]. Based on the ISO standard, when a hemolysis index of a substance is less than 5%, it is considered safe[71]. The hemolytic assay on human erythrocytes was performed on the synthesized CTT-CS/SF/$Mg(OH)_2$ nanobiocomposite scaffold to determine its hemolysis potency (Fig. 8a–b). According to the obtained results, it was found that the synthesized scaffold had a very poor hemolytic activity of about 4.5%, while Triton X-100 lysed almost RBCs as a positive control. Also, in this test, 0.9% NaCl solution was used as negative control with hemolytic activity of about 1.2%. It should be noted that the reported results are the mean of 3 independent experiments. Various studies have shown that chitosan-based hydrogels are compatible with blood[71]. As well as, silk fibroin-based scaffolds do not have high hemolysis potential[72]. However, it has been determined that $Mg(OH)_2$ NPs have a mild hemolytic activity[39]. Apart from the mentioned results, it was showed that there was no significant difference between the hemolysis percentage of CTT-CS hydrogel (3.6%), CTT-CS/SF hydrogel (4%), and CTT-CS/SF/$Mg(OH)_2$ nanobiocomposite scaffold (4.5%) (Fig. 8a). Therefore, the addition of SF and $Mg(OH)_2$ NPs to the structure of CTT-CS hydrogel were not accompanied by distinctive changes in hemolytic activity. On the whole, it can be concluded that the CTT-CS/SF/$Mg(OH)_2$ nanobiocomposite scaffold is biocompatible with blood and it can be considered in tissue engineering and wound healing.

Inhibition of anti-biofilm activity results. After washing the biofilms from the samples, the absorbance of the resulting solutions was measured at 570 nm in the 96 micro-well plate. As could be seen in Fig. 9a–b, the OD value of polystyrene, CTT-CS hydrogel and CTT-CS/SF/$Mg(OH)_2$ nanobiocomposite scaffold pieces, was 0.88, 0.32 and 0.11, respectively. According to the statistical analysis, the anti-biofilm activity of the CTT-CS/SF/$Mg(OH)_2$ nanobiocomposite scaffold fragment was significantly lower than the CTT-CS hydrogel and poly-

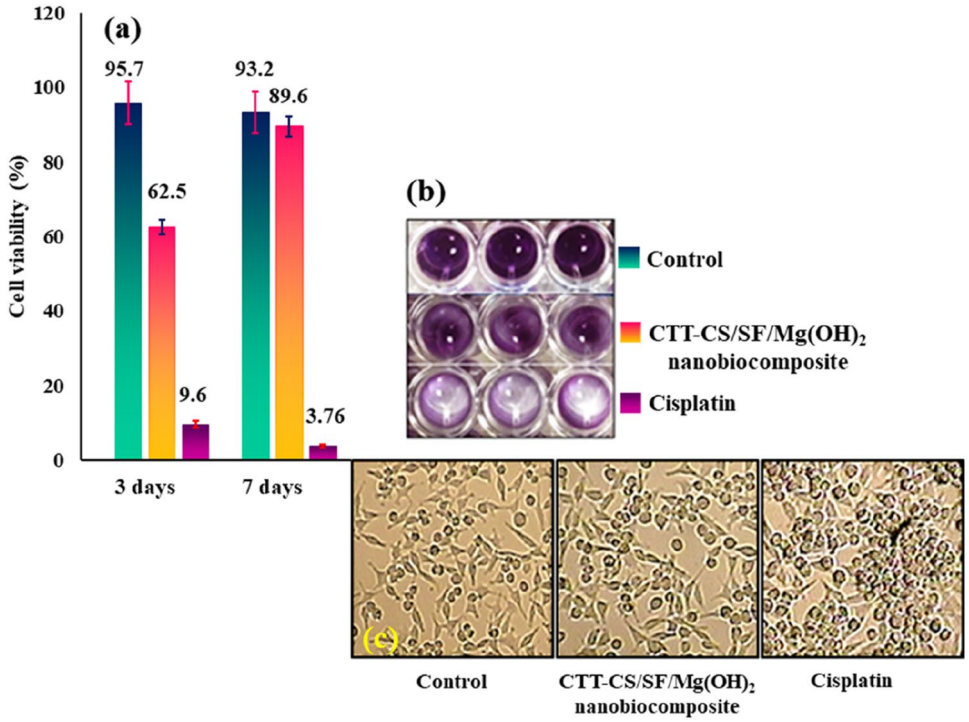

Figure 7. (**a**) Cell viability histogram of untreated Hu02 cells as control, CTT-CS/SF/$Mg(OH)_2$ nanobiocomposite scaffold and cisplatin treatments at 3 days and 7 days, (**b**) image of microplate well from MTT assay on Hu02 cell line, (**c**) inverted microscope images of untreated cells as control, CTT-CS/SF/$Mg(OH)_2$ nanobiocomposite scaffold and cisplatin treatments.

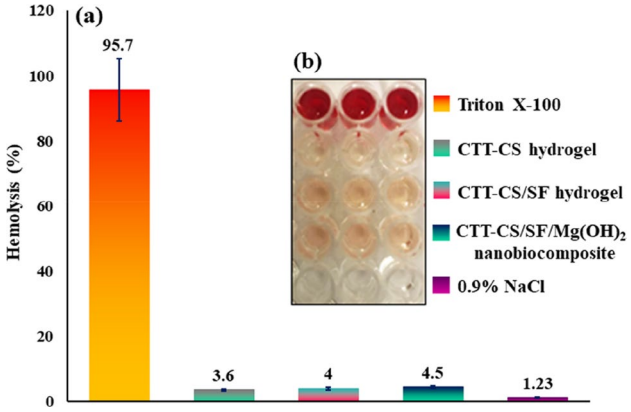

Figure 8. (**a**,**b**) Hemolysis histogram and 96-well plate image of Triton X-100 (positive control), CTT-CS hydrogel, CTT-CS/SF hydrogel, CTT-CS/SF/$Mg(OH)_2$ nanobiocomposite scaffold, and 0.9% NaCl (negative control).

styrene pieces ($p < 0.05$). In fact, the decrease in OD of the NB culture medium containing scaffold at 570 nm, indicated that the synthesized scaffold could well prevent the *P. aeruginosa* biofilm formation on its surface. It should be noted that chitosan is a potent antimicrobial and non-toxic biopolymer which, its antimicrobial property is due to its cationic nature[11]. Antimicrobial activity of this substance has been observed against various microorganisms such as bacteria, fungi and algae[73]. Therefore, chitosan and its modified derivatives have become one of the favorite antimicrobial materials for wound dressing[28]. In addition to this, many studies have shown that $Mg(OH)_2$ NPs have antibacterial properties[74]. Overall, it can be concluded that the addition and presence of $Mg(OH)_2$ NPs in the structure of designed synthesized nanobiocomposite scaffold could enhance its antimicrobial activity. Following that, owning this property could extend its biomedical potential in different fields such as tissue engineering and wound healing.

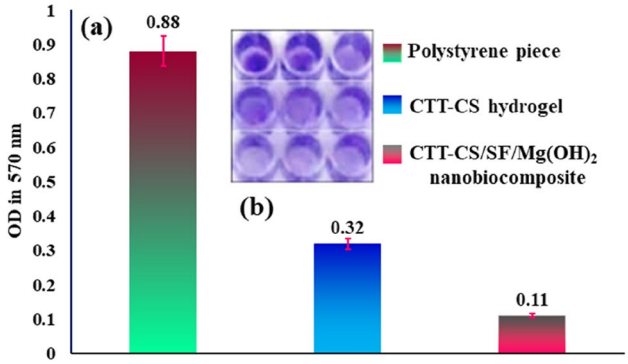

Figure 9. (**a**,**b**) Anti-biofilm histogram and 96-well plate image of polystyrene piece, CTT-CS hydrogel, CTT-CS/SF/$Mg(OH)_2$ nanobiocomposite. It was clear that synthesized nanobiocomposite scaffold was able to inhibit the *P. aeruginosa* biofilm formation.

Conclusion

As summery, given the importance of regenerative medicine strategies and dynamic wound healing approaches, novel CTT-CS/SF/$Mg(OH)_2$ nanobiocomposite scaffold was designed and synthesized according to modifying CTT-CS hydrogel using extracted SF and $Mg(OH)_2$ nanoparticles. The modification processes of CTT-CS hydrogel substrate and the formation of this new nanobiocomposite scaffold were accompanied by remarkable and eye-catching biological features. In order to explain more, based on the MTT assay studies after 3 days and 7 days, the cell viability of CTT-CS/SF/$Mg(OH)_2$ nanobiocomposite scaffold was 62.5% and 89.6% respectively. These results demonstrated that the cell viability increased with the time. This increment in cell viability could express the biocompatibility of CTT-CS/SF/$Mg(OH)_2$ nanobiocomposite scaffold. Following that, given the hemolytic assay results, there was not observed any particular difference in hemolysis percentage of CTT-CS hydrogel (3.6%), CTT-CS/SF hydrogel (4%), and CTT-CS/SF/$Mg(OH)_2$ nanobiocomposite scaffold (4.5%). Besides, it was indicated that in comparison to CTT-CS hydrogel and as well, due to the statistical analysis and OD values, the anti-biofilm activity of the CTT-CS/SF/$Mg(OH)_2$ nanobiocomposite scaffold was significantly high and it could well inhibit the *P. aeruginosa* biofilm formation on its surface. Furthermore, apart from the structural characteristics (FT-IR, EDX, FE-SEM, TG analyses), the addition of SF and $Mg(OH)_2$ NPs could enhance the compressive strength from 65.42 to 649.56 kPa. Bearing in mind theses structural characteristics and biological assays, this novel nanobiocomposite scaffold could be considered more in wound healing use.

Received: 8 August 2020; Accepted: 17 December 2020
Published online: 12 January 2021

References

1. Gonzalez, A. C. O., Costa, T. F., Andrade, Z. A. & Medrado, A. R. A. P. Wound healing—A literature review. *An. Bras. Dermatol.* **91**, 614–620 (2016).
2. MacEwan, M. R., MacEwan, S., Kovacs, T. R. & Batts, J. What makes the optimal wound healing material? A review of current science and introduction of a synthetic nanofabricated wound care scaffold. *Cureus* **9**, e1736 (2017).
3. Asgharnasl, S., Eivazzadeh-Keihan, R., Radinekiyan, F. & Maleki, A. Preparation of a novel magnetic bionanocomposite based on factionalized chitosan by creatine and its application in the synthesis of polyhydroquinoline, 1,4-dyhdropyridine and 1,8-dioxo-decahydroacridine derivatives. *Int. J. Biol. Macromol.* **144**, 29–46 (2020).
4. Maleki, A., Panahzadeh, M. & Eivazzadeh-keihan, R. Agar: A natural and environmentally-friendly support composed of copper oxide nanoparticles for the green synthesis of 1,2,3-triazoles. *Green Chem. Lett. Rev.* **12**, 395–406 (2019).
5. Sarker, B. *et al.* Fabrication of alginate–gelatin crosslinked hydrogel microcapsules and evaluation of the microstructure and physico-chemical properties. *J. Mater. Chem. B.* **2**, 1470–1482 (2014).
6. Vasile, C., Pamfil, D., Stoleru, E. & Baican, M. New developments in medical applications of hybrid hydrogels containing natural polymers. *Molecules* **25**, 1539 (2020).
7. Caló, E. & Khutoryanskiy, V. V. Biomedical applications of hydrogels: A review of patents and commercial products. *Eur. Polym. J.* **65**, 252–267 (2015).
8. Kamoun, E. A., Kenawy, E. R. S. & Chen, X. A review on polymeric hydrogel membranes for wound dressing applications: PVA-based hydrogel dressings. *J. Adv. Res.* **8**, 217–233 (2017).
9. Da, L. C., Huang, Y. Z. & Xie, H. Q. Progress in development of bioderived materials for dermal wound healing. *Regen. Biomater.* **4**, 325–334 (2017).
10. Hamdi, M. *et al.* A novel blue crab chitosan/protein composite hydrogel enriched with carotenoids endowed with distinguished wound healing capability: *In vitro* characterization and *in vivo* assessment. *Mater. Sci. Eng. C* **113**, 110978 (2020).
11. Ahmed, S. & Ikram, S. Chitosan based scaffolds and their applications in wound healing. *Achieve Life Sci.* **10**, 27–37 (2016).
12. Dai, T., Tanaka, M., Huang, Y. Y. & Hamblin, M. R. Chitosan preparations for wounds and burns: Antimicrobial and wound-healing effects. *Expert Rev. Anti-infect. Ther.* **9**, 857–879 (2011).
13. Reza, G., Shahin, N. P., Tahereh, T. M. & Javad, H. S. M. Synergistic antibacterial activity and wound healing properties of selenium-chitosan-mupirocin nanohybrid system: An *in vivo* study on rat diabetic *Staphylococcus aureus* wound infection model. *Sci. Rep.* **10**, 1–10 (2020).
14. Shariatinia, Z. & Jalali, A. M. Chitosan-based hydrogels: Preparation, properties and applications. *Int. J. Biol. Macromol.* **115**, 194–220 (2018).
15. Eivazzadeh-Keihan, R. *et al.* Recent progress in optical and electrochemical biosensors for sensing of *Clostridium* botulinum neurotoxin. *TrAC Trends Anal. Chem.* **103**, 184–197 (2018).

16. Mohammadinejad, A. *et al.* Development of biosensors for detection of alpha-fetoprotein: As a major biomarker for hepatocellular carcinoma. *TrAC Trends Anal. Chem.* **130**, 115961 (2020).
17. Eivazzadeh-Keihan, R. *et al.* Carbon based nanomaterials for tissue engineering of bone: Building new bone on small black scaffolds: A review. *J. Adv. Res.* **18**, 185–201 (2019).
18. Cheung, R. C. F., Ng, T. B., Wong, J. H. & Chan, W. Y. Chitosan: An update on potential biomedical and pharmaceutical applications. *Mar. Drugs* **13**, 5156–5186 (2015).
19. Zhou, Z., Lin, S., Yue, T. & Lee, T. C. Adsorption of food dyes from aqueous solution by glutaraldehyde cross-linked magnetic chitosan nanoparticles. *J. Food Eng.* **126**, 133–141 (2014).
20. Pujana, M. A., Pérez-Álvarez, L., Iturbe, L. C. C. & Katime, I. Biodegradable chitosan nanogels crosslinked with genipin. *Carbohydr. Polym.* **94**, 836–842 (2013).
21. Wang, Y. *et al.* Chitosan cross-linked poly(acrylic acid) hydrogels: Drug release control and mechanism. *Colloids Surf. B.* **152**, 252–259 (2017).
22. Zeng, M., Yuan, X., Yang, Z. & Qi, C. Novel macroporous palladium cation crosslinked chitosan membranes for heterogeneous catalysis application. *Int. J. Biol. Macromol.* **68**, 189–197 (2014).
23. Depan, D. & Singh, R. P. *Surface Modification of Chitosan and Its Implications in Tissue Engineering and Drug Delivery* 20–44 (Wiley, New York, 2015).
24. Gomes, S., Leonor, I. B., Mano, J. F., Reis, R. L. & Kaplan, D. L. Natural and genetically engineered proteins for tissue engineering. *Prog. Polym. Sci.* **37**, 1–17 (2012).
25. Bani, M. S. *et al.* Casein-coated iron oxide nanoparticles for *in vitro* hyperthermia for cancer therapy. *Spin.* **9**, 1940003 (2019).
26. Chun, H. J., Park, K., Kim, C. H. & Khang, G. In *Novel Biomaterials for Regenerative Medicine* (eds Chun, H. J. *et al.*) (Springer, New York, 2018).
27. Ju, H. W. *et al.* Wound healing effect of electrospun silk fibroin nanomatrix in burn-model. *Int. J. Biol. Macromol.* **85**, 29–39 (2016).
28. Guang, S. *et al.* Chitosan/silk fibroin composite scaffolds for wound dressing. *J. Appl. Polym. Sci.* **132**, 42503–42510 (2015).
29. Keirouz, A. *et al.* High-throughput production of silk fibroin-based electrospun fibers as biomaterial for skin tissue engineering applications. *Mater. Sci. Eng. C.* **112**, 110939 (2020).
30. Ribeiro, V. P., Pina, S., Oliveira, J. M. & Reis, R. L. In *Silk Fibroin-Based Hydrogels and Scaffolds for Osteochondral Repair and Regeneration* (eds Ribeiro, V. P. *et al.*) 305–325 (Springer, New York, 2018).
31. Nguyen, T. P. *et al.* Silk fibroin-based biomaterials for biomedical applications: A review. *Polymers* **11**, 1933 (2019).
32. Balan, K. K. & Sundaramoorthy, S. Hydroentangled nonwoven eri silk fibroin scaffold for tissue engineering applications. *J. Ind. Text.* **48**, 1291–1309 (2019).
33. Selvaraj, S. & Fathima, N. N. Fenugreek., Incorporated silk fibroin nanofibers—A potential antioxidant scaffold for enhanced wound healing. *ACS Appl. Mater. Interfaces* **9**, 5916–5926 (2017).
34. Cengiz, I. F. *et al.* Suturable regenerated silk fibroin scaffold reinforced with 3D-printed polycaprolactone mesh: Biomechanical performance and subcutaneous implantation. *J. Mater. Sci. Mater. Med.* **30**, 63 (2019).
35. Wang, S. D., Ma, Q., Wang, K. & Chen, H. W. Improving antibacterial activity and biocompatibility of bioinspired electrospinning silk fibroin nanofibers modified by graphene oxide. *ACS Omega* **3**, 406–413 (2018).
36. Cui, B. *et al.* Collagen-tussah silk fibroin hybrid scaffolds loaded with bone mesenchymal stem cells promote skin wound repair in rats. *Mater. Sci. Eng. C* **109**, 110611 (2020).
37. Calamak, S. *et al.* Ag/silk fibroin nanofibers: Effect of fibroin morphology on Ag^{+} release and antibacterial activity. *Eur. Polym. J.* **67**, 99–112 (2015).
38. De Simone, S., Gallo, A., Paladini, F., Sannino, A. & Pollini, M. Development of silver nano-coatings on silk sutures as a novel approach against surgical infections. *J. Mater. Sci. Mater. Med.* **25**, 2205–2214 (2014).
39. Zhou, W., Qiao, X. L., Zhang, L., Guo, J. Y. & Zheng, J. Synthesis and hemolytic activity of magnesium hydroxide nanoparticles. *J. Adv. Mater. Res.* **971**, 228–231 (2014).
40. Halbus, A. F., Horozov, T. S. & Paunov, V. N. Controlling the antimicrobial action of surface modified magnesium hydroxide nanoparticles. *Biomimetics* **4**, 41 (2019).
41. Martin, P. D., Schneck, D. W., Dane, A. L. & Warwick, M. J. The effect of a combination antacid preparation containing aluminium hydroxide and magnesium hydroxide on rosuvastatin pharmacokinetics. *Curr. Med. Res. Opin.* **24**, 1231–1235 (2008).
42. Scott, G. *et al.* Lack of effect of omeprazole or of an aluminium hydroxide/magnesium hydroxide antacid on the pharmacokinetics of lumiracoxib. *Clin. Pharmacokinet.* **43**, 341–348 (2004).
43. Tong, K., Song, X., Xiao, G. & Yu, J. Colloidal processing of $Mg(OH)_2$ aqueous suspensions using sodium polyacrylate as dispersant. *Ind. Eng. Chem. Res.* **53**, 4755–4762 (2014).
44. Waaijers, S. L. *et al.* In *Reviews of Environmental Contamination and Toxicology* (eds Waaijers, S. L. *et al.*) 1–71 (Springer, New York, 2013).
45. Eivazzadeh-Keihan, R., Radinekiyan, F., Madanchi, H., Aliabadi, H. A. M. & Maleki, A. Graphene oxide/alginate/silk fibroin composite as a novel bionanostructure with improved blood compatibility, less toxicity and enhanced mechanical properties. *Carbohydr. Polym.* **248**, 116802 (2020).
46. Bhardwaj, N. & Kundu, S. C. Silk fibroin protein and chitosan polyelectrolyte complex porous scaffolds for tissue engineering applications. *Carbohydr. Polym.* **85**, 325–333 (2011).
47. Gholipourmalekabadi, M. *et al.* Development of a cost-effective and simple protocol for decellularization and preservation of human amniotic membrane as a soft tissue replacement and delivery system for bone marrow stromal cells. *Adv. Healthc. Mater.* **4**, 918–926 (2015).
48. Archana, D., Singh, B. K., Dutta, J. & Dutta, P. *In vivo* evaluation of chitosan–PVP–titanium dioxide nanocomposite as wound dressing material. *Carbohydr. Polym.* **95**, 530–539 (2013).
49. Haney, E. F., Trimble, M. J., Cheng, J. T., Vallé, Q. & Hancock, R. E. Critical assessment of methods to quantify biofilm growth and evaluate antibiofilm activity of host defence peptides. *Biomolecules* **8**, 29 (2018).
50. Mohamed, N. A. & Al-mehbad, N. Y. Novel terephthaloyl thiourea cross-linked chitosan hydrogels as antibacterial and antifungal agents. *Int. J. Biol. Macromol.* **57**, 111–117 (2013).
51. Eivazzadeh-Keihan, R. *et al.* A novel biocompatible core-shell magnetic nanocomposite based on cross-linked chitosan hydrogels for in vitro hyperthermia of cancer therapy. *Int. J. Biol. Macromol.* **140**, 407–414 (2019).
52. Atrian, M., Kharaziha, M., Emadi, R. & Alihosseini, F. Silk-laponite fibrous membranes for bone tissue engineering. *Appl. Clay Sci.* **174**, 90–99 (2019).
53. Wang, H. Y. & Zhang, Y. Q. Processing and characterisation of a novel electropolymerized silk fibroin hydrogel membrane. *Sci. Rep.* **4**, 6182 (2014).
54. Stefanis, E. & Panayiotou, C. Deacidification of documents containing iron gall ink with dispersions of $Ca(OH)_2$ and $Mg(OH)_2$ nanoparticles. *Restaurator* **31**, 19–40 (2010).
55. Mehrabani, M. G. *et al.* Chitin/silk fibroin/TiO_2 bio-nanocomposite as a biocompatible wound dressing bandage with strong antimicrobial activity. *Int. J. Biol. Macromol.* **116**, 966–976 (2018).
56. Fernandes Queiroz, M., Melo, K. R. T., Sabry, D. A., Sassaki, G. L. & Rocha, H. A. O. Does the use of chitosan contribute to oxalate kidney stone formation?. *Mar. Drugs* **13**, 141–158 (2015).

57. Ha, S. W., Tonelli, A. E. & Hudson, S. M. Structural studies of *Bombyxmori* silk fibroin during regeneration from solutions and wet fiber spinning. *Biomacromol* **6**, 1722–1731 (2005).
58. Ansari, A., Ali, A. & Asif, M. Microwave-assisted MgO NP catalyzed one-pot multicomponent synthesis of polysubstituted steroidal pyridines. *New J. Chem.* **42**, 184–197 (2018).
59. Freddi, G., Monti, P., Nagura, M., Gotoh, Y. & Tsukada, M. Structure and molecular conformation of tussah silk fibroin films: Effect of heat treatment. *J. Polym. Sci. Pol. Phys.* **35**, 841–847 (1997).
60. Gupta, P. *et al.* Mimicking form and function of native small diameter vascular conduits using mulberry and non-mulberry patterned silk films. *ACS Appl. Mater. Interfaces* **8**, 15874–15888 (2016).
61. Masheane, M. *et al.* Antimicrobial properties of chitosan-alumina/f-MWCNT nanocomposites. *J. Nanotechnol.* **2016**, 8 (2016).
62. Gu, J. & Catchmark, J. M. Roles of xyloglucan and pectin on the mechanical properties of bacterial cellulose composite films. *Cellulose* **21**, 275–289 (2014).
63. Gu, Y. *et al.* Chitosan/silk fibroin-based, Schwann cell-derived extracellular matrix-modified scaffolds for bridging rat sciatic nerve gaps. *Biomaterials* **35**, 2253–2263 (2014).
64. Jayakumar, R., Prabaharan, M., Kumar, P. S., Nair, S. & Tamura, H. Biomaterials based on chitin and chitosan in wound dressing applications. *Biotechnol. Adv.* **29**, 322–337 (2011).
65. Zhang, Q., Tian, M., Wu, Y., Lin, G. & Zhang, L. Effect of particle size on the properties of $Mg(OH)_2$-filled rubber composites. *J. Appl. Polym. Sci.* **94**, 2341–2346 (2004).
66. Niamsa, N., Srisuwan, Y., Baimark, Y., Phinyocheep, P. & Kittipoom, S. Preparation of nanocomposite chitosan/silk fibroin blend films containing nanopore structures. *Carbohydr. Polym.* **78**, 60–65 (2009).
67. Shankar, S., Tanomrod, N., Rawdkuen, S. & Rhim, J. W. Preparation of pectin/silver nanoparticles composite films with UV-light barrier and properties. *Int. J. Biol. Macromol.* **92**, 842–849 (2016).
68. Rahmani Del Bakhshayesh, A. *et al.* Recent advances on biomedical applications of scaffolds in wound healing and dermal tissue engineering. *Artif. Cell. Nanomed. B.* **46**, 691–705 (2018).
69. Meng, N. *et al.* Nano-$Mg(OH)_2$-induced proliferation inhibition and dysfunction of human umbilical vein vascular endothelial cells through caveolin-1-mediated endocytosis. *Cell. Biol. Toxicol.* **31**, 15–27 (2015).
70. Elahi, M. F., Guan, G. & Wang, L. Hemocompatibility of surface modified silk fibroin materials: A review. *Rev. Adv. Mater. Sci.* **38**, 148–159 (2014).
71. Zhou, H. Y., Zhang, Y. P., Zhang, W. F. & Chen, X. G. Biocompatibility and characteristics of injectable chitosan-based thermosensitive hydrogel for drug delivery. *Carbohydr. Polym.* **83**, 1643–1651 (2011).
72. Andiappan, M. *et al.* Electrospun eri silk fibroin scaffold coated with hydroxyapatite for bone tissue engineering applications. *Prog. Biomater.* **2**, 6 (2013).
73. Ahmed, S. & Ikram, S. Chitosan and its derivatives: A review in recent innovations. *Int. J. Pharm. Sci. Res.* **6**, 14 (2015).
74. Dong, C. *et al.* Investigation of $Mg(OH)_2$ nanoparticles as an antibacterial agent. *J. Nanopart. Res.* **12**, 2101–2109 (2010).

Acknowledgements

The authors gratefully acknowledge the partial support from the Research Council of the Iran University of Science and Technology.

Author contributions

R.E., F.R., H.A., S.S., B.T. and H.M. wrote the main manuscript text. A.M. revised the MS and supervised all the process. All authors reviewed the manuscript.

Competing interests

The authors declare no competing interests.

Additional information

Correspondence and requests for materials should be addressed to A.M. or H.M.

Reprints and permissions information is available at www.nature.com/reprints.

Publisher's note Springer Nature remains neutral with regard to jurisdictional claims in published maps and institutional affiliations.